



**HAL**  
open science

## Diffraction grating enhanced photoluminescence from etching-free erbium thin films

A. Gassenq, H-S Nguyen, E. Cleyet-Merle, Sébastien Cueff, A. Pereira

► **To cite this version:**

A. Gassenq, H-S Nguyen, E. Cleyet-Merle, Sébastien Cueff, A. Pereira. Diffraction grating enhanced photoluminescence from etching-free erbium thin films. *Optics Letters*, 2023, 48 (11), pp.2893. 10.1364/OL.486893 . hal-04115684

**HAL Id: hal-04115684**

**<https://hal.science/hal-04115684>**

Submitted on 2 Jun 2023

**HAL** is a multi-disciplinary open access archive for the deposit and dissemination of scientific research documents, whether they are published or not. The documents may come from teaching and research institutions in France or abroad, or from public or private research centers.

L'archive ouverte pluridisciplinaire **HAL**, est destinée au dépôt et à la diffusion de documents scientifiques de niveau recherche, publiés ou non, émanant des établissements d'enseignement et de recherche français ou étrangers, des laboratoires publics ou privés.

# Diffraction grating enhanced photoluminescence from etching-free erbium thin films

A. GASSENQ,<sup>1,\*</sup> H-S NGUYEN,<sup>2</sup> E. CLEYET-MERLE,<sup>1</sup> S. CUEFF,<sup>2</sup> A. PEREIRA,<sup>1</sup>

<sup>1</sup> Université de Lyon, Institut Lumière Matière, UCBL, CNRS, UMR5306, F-69622, LYON, France.

<sup>2</sup> Institut des Nanotechnologies de Lyon, UMR 5270, CNRS, ECL, INSA, UCBL, F-69134, LYON, France

\*Corresponding author: [alban.gasseng@univ-lyon1.fr](mailto:alban.gasseng@univ-lyon1.fr)

Received 10 February 2023; revised 21 April 2023; accepted 26 April 2023; posted 28 April 2023; published <https://doi.org/10.1364/OL.486893>

Micro-structuration by etching is commonly used in integrated optics, adding complex and costly processing steps which can also potentially damage the devices performances due to the degradation of the etched sidewalls. For diffraction grating fabrication, different strategies have been developed to avoid etching, like layer deposition on structured surface or grating deposition on top of active layers. However, etching remains one of the best process for making high aspect ratio diffraction grating. In this work, we have developed fully structured diffraction gratings (i.e. like fully etched gratings) using lift-off based processing performed in pulsed laser deposited layers since the combination of both techniques is of great interest for making microstructures without etching. We have first studied the influence of the lithography doses in the lift-off process, showing that (1) micrometric spatial resolution can be achieved and (2) sidewall angle can be controlled from 50 to 150° in 0.5 μm thick layers. Using such optimizations, we have then fabricated Er-doped Y<sub>2</sub>O<sub>3</sub> uniaxial diffraction gratings with different periods ranging from 3 to 8 μm. The fabricated devices exhibit emission and reflectivity properties as a function of the collection angle in good agreement with the modeling with a maximum luminescence enhancement of x15 compared to an unstructured layer at a wavelength of 1.54 μm. This work highlights thus the lift-off based processing combined with pulsed laser deposition as a promising technique for etch-free practical applications such as luminescence enhancement in Er doped layers.

## 1. INTRODUCTION

Material etching is a standard process in photonics for the fabrication of a large variety of micro-devices like waveguides, lasers, photo-detectors gratings, and so on. It consists of the ablation of a surface through a micro-structured mask (e.g photoresist). Such a processing step remains complicated, expensive and potentially detrimental for practical applications since it can also induce extra-losses due to the degradation of materials along etched sidewalls[1,2] as well as undesired roughness. For instance, grating devices are widely spread in photonics for light coupling [3], filters [4], mirror definitions [5] and so on. Furthermore, luminescence enhancement by diffraction grating is also very interesting to increase the spontaneous emission, to control the light direction or to increase the pump absorption[6–11]. For that purpose, different strategies have been developed to avoid etching in the emissive layer like using diffraction elements below[6–8,12] or above the active layer[9,10], but these methods cannot be used to fully structure the emitting layers (like the fully etched gratings compared to the shallow etched gratings). For rare earth doped materials, etching is also commonly used in photonics[13–17]. Other methods have also been studied for integration but with millimetric resolution[18,19], without structuration[10,20,21], using ion beam[22–24], or by layer deposition on pre-structured substrates[25,26]. Indeed, rare earth emitters have recently growing as a very interesting emerging platform

for quantum photonics [27,28] due to the lanthanide high coherences[29] allowing to realize many quantum functions like sources[16], spin readout[17,24], memories[22], microwave transducers[23] and so on. Therefore, developing diffraction gratings with rare earth emitters without etching is of great interest to control the light emission of such layers for different applications like laser integration[20,30] with grating, signal processing[31], quantum optics[27,28], and so on.

In this work, we have fabricated Er<sup>3+</sup> rare-earth-doped gratings by Pulsed Laser Deposition (PLD) and lift-off processing without etching. Lift-off processing is usual in microelectronics but is limited to low thermal budget layers[32,33] and can also induce high sidewall roughness[34]. Since PLD deposition can provide high quality films at low temperature deposition due to the high kinetic energy of the atoms during deposition[35], it is thus a compatible technique with the lift-off processing to fabricate thicker micro-devices without etching[36]. However, low roughness and high-resolution patterning in thick layer are relatively challenging with lift-off processing. For that purpose, we have first investigated the lithography dose influence in the shape of the microstructure to determine the minimum resolution size. We have then fabricated diffraction gratings with different periods and measured their emission and reflection properties as a function of the wavevector. Structured layers exhibit a controlled angular-dependence in emission, in good agreement with theory and a strong luminescence enhancement at certain angles. This work thus shows that the lift-off

processing combined with PLD is a relevant approach for etch-free fabrication of practical photonic devices like diffraction gratings as future building blocks in many applications in integrated optics like rare-earth ions based quantum nanophotonics.[27]

## 2. GRATTING

### A. Description

Our reference design consists of 0.6  $\mu\text{m}$  thick  $\text{Y}_2\text{O}_3:\text{Er}^{3+}$  layer on  $\text{SiO}_2$  with 1.87 [37] and 1.44 [38] refractive index at 1.54  $\mu\text{m}$  wavelength, respectively. This structure corresponds to a single-mode waveguide slab in the infrared spectral window 1.3-1.8  $\mu\text{m}$ . Most of  $\text{Y}_2\text{O}_3:\text{Er}^{3+}$  emission radiates into this guided mode and is trapped within the slab due to total internal reflection, while only  $\sim 8\%$  percent of the emitted light may escape to the air. To enhance light extraction and absorption, a periodic corrugation of period  $p$  is introduced (see Figure 1-a). This modulation diffracts the initial guided mode and induces a band folding effect: each diffraction order  $m$  implements a wavevector-shift of  $K_m=2m\pi/p$  to the dispersion of the initial guided mode. As a consequence, for certain values of diffraction order  $m$ , the folded guided mode is brought above the light-line and becomes guided mode resonances (GMR). The GMRs are out-coupling channels for  $\text{Y}_2\text{O}_3:\text{Er}^{3+}$  guided emission and the angular pattern of emitted light is dictated by the dispersion of the GMRs. At first approximation, when only the bandfolding mechanism is taken into account, the dispersion of GMRs can be analytically calculated.

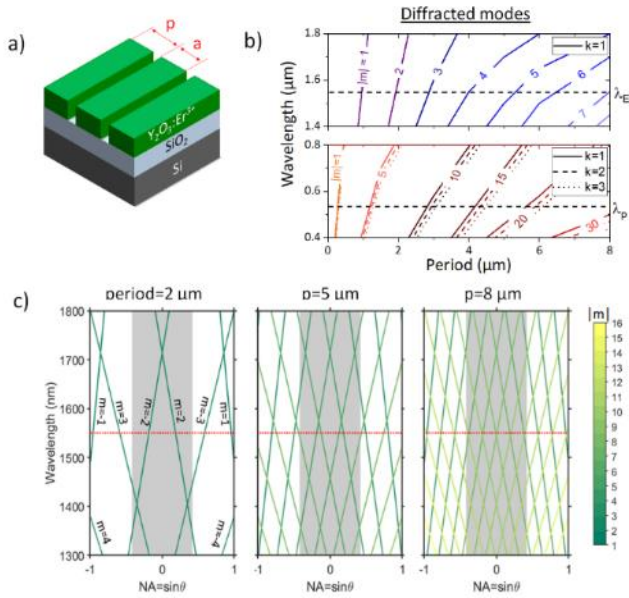


FIG. 1: Diffraction grating modeling with (a) used parameters, (b) mode position as a function of the period around  $\lambda_{\text{Er}}=1.54 \mu\text{m}$  (top) and  $\lambda_p=0.532 \mu\text{m}$  (bottom) wavelength and (c) calculated dispersion of GMRs.

### B. Modeling

Figure 1-c presents calculated GMR dispersions for the 1.3-1.8  $\mu\text{m}$  wavelength ranges, with three different periods 2, 5 and 8  $\mu\text{m}$ . The red dashed line corresponds to the wavelength at which the erbium emission is maximal ( $\lambda_{\text{Er}}=1.54 \mu\text{m}$  for the  $^4\text{I}_{13/2} \rightarrow ^4\text{I}_{15/2}$  transition of  $\text{Er}^{3+}$ ). The gray shading region indicates the numerical aperture in our experimental setup ( $\text{NA}=0.42$ ) studied later in this work. For a small period of  $p=2\mu\text{m}$ , we “only” have eight GMRs corresponding to

diffraction orders  $m=\pm 1, \pm 2, \pm 3, \pm 4$ . When limited within a numerical aperture  $\text{NA}=0.42$  and focusing in the vicinity of erbium emission wavelength at 1.54 $\mu\text{m}$ , only two GMRs of  $m= \pm 2$  exists for 2  $\mu\text{m}$  period which are responsible of the extraction of erbium emission to free space. However, for big periods, many more GMRs are present, and the light extraction mechanism involves multi channels. Similar arguments can be applied for the enhancement of absorption mechanisms in the visible range ( $\lambda_p=0.532 \mu\text{m}$  for the  $^4\text{I}_{15/2} \rightarrow ^2\text{H}_{11/2}$  transition of  $\text{Er}^{3+}$ ). In that case, the waveguide is already multimode transverse in the visible range, thus the number of GMRs in the visible range is much more important (bandfolding for different guided modes, with different diffraction orders). Therefore, the mode positions have been summarized as a function of the period at  $0^\circ$  on the Figure 1-b around the  $\text{Er}^{3+}$  extracted emission ( $\lambda=1.54 \mu\text{m}$  for the  $^4\text{I}_{13/2} \rightarrow ^4\text{I}_{15/2}$  transition) and absorption ( $\lambda_p=0.532 \mu\text{m}$  for the  $^4\text{I}_{15/2} \rightarrow ^2\text{H}_{11/2}$  transition) which will be experimentally studied later in this work. We clearly see that the lower period absorbs at lower diffraction mode (with different transverse modes  $k=1, 2$  or 3) and that the emission is mono-mode (with only one transverse mode  $k=1$ ).

## 3. FABRICATION

### A. Processing

Figure 2 presents the used process flow for the grating fabrication. Micro-strips were first patterned with AZ5214 photoresist previously spin coated on top of 2  $\mu\text{m}$  thick  $\text{SiO}_2$  layer on Si with a laser writer using GDS files. Different exposure doses were investigated, whereas the development time was kept constant at 60 s. A 500 nm-thick  $\text{Y}_2\text{O}_3:\text{Er}^{3+}$  (1 at. %) layer was then deposited on top of the structured substrate with a KrF excimer laser ( $\lambda=248 \text{ nm}$ ,  $t=17 \text{ ns}$ , Coherent Compex Pro) operating at 5 Hz. The laser beam was focused on the target over 2  $\text{mm}^2$ , and the laser energy and the  $\text{Y}_2\text{O}_3:\text{Er}^{3+}$  substrate distance were kept constant at 73 mJ and 6 cm, respectively. Substrate rotation was used to obtain homogeneous layer thickness at a growth speed of 3.5 nm/min. The film was grown at room temperature in an oxygen-gas atmosphere (10-3 mbar). Lift-off was then performed in ultrasonic wet bench with acetone. After the lift-off, samples were annealed for 24 h at 650  $^\circ\text{C}$  in order to activate the doping and to improve the structural quality of the film [36].

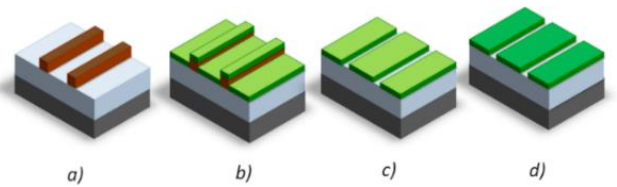


FIG. 2: Process flow for the grating fabrication using a) lithography of photoresist, b)  $\text{Y}_2\text{O}_3:\text{Er}^{3+}$  PLD, c) lift-off and d) annealing

### B. Dose influence

Figure 3-a presents the influence of the lithography dose before and after the lift-off processing (corresponding to the process step in Figure 2-b and 2-c) with SEM (Scanning Electron Microscopy) images. SEM images were taken at  $45^\circ$  angle tilt with a TESCAN SEM at 5 kV with a secondary electron detector. Low doses were obtained with negative photoresist and high doses with positive photoresist using AZ5214E[Eu] reversible photoresist from micro-chemicals company, in order to control the slope angle of the photoresist [39]. By comparing the imaging before and after lift-off, we clearly see that the PLD layer

follows the lithography shape. Figure 3-b plots the slope  $\theta$  angle of the microstructure and the pattern width difference  $\Delta a$  (see inset of the Figure 3-b) as a function of the lithography dose. This width difference corresponds to the absolute difference of the pattern size compared to the theoretical width ( $a$  in the Figure 1-a), which was used in the GDS file and sent to the laser lithography. For negative photoresist, the pattern increases with the dose since it remains on the sample after exposure (i.e. negative mode). For positive photoresist, the dimension of the developed pattern decreases with the dose since the exposed region is removed from the sample after exposure (i.e. positive mode). Regarding the shape of the devices, the obtained microstructures have a sidewall angle ranging from  $50^\circ$  to  $150^\circ$ . For positive photoresist, the sidewall angle is below  $90^\circ$  with higher roughness coming from the breaking of the layer during the lift-off. For negative photoresist, low roughness is observed since the deposited material is not in contact with the photoresist, especially for the lowest dose. These behaviors come from the reversible nature of the used photoresist AZ5214. Therefore, the exposure dose is a primordial parameter which needs to be controlled as a function of the targeted shape. The Figure 3-c presents two examples of extrema for the minimum and maximum angles we can obtain on a disk. In that case, we observe here “bowl” (for low dose with negative photoresist) or “pancake” (for high dose with positive photoresist) shapes which confirms that we can obtain atypical shapes and very low roughness (for low dose) with this technique. Indeed, as it can be seen in the SEM images after liftoff for low dose in the Figure 2-a, the sidewall roughness is in the same order of magnitude than the roughness of the unstructured part of the layer.

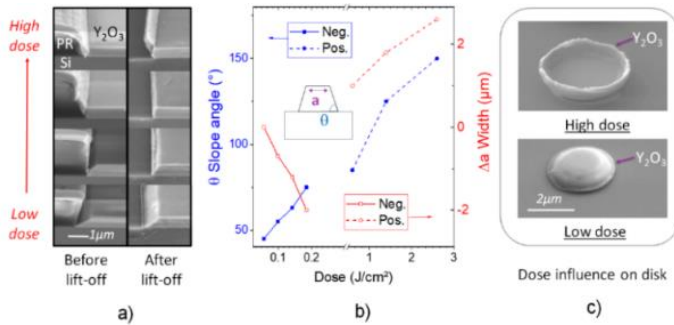


FIG. 3: Influence of the lithography dose on the shape of the microstructure with a) SEM tilted imaging before and after lift-off; b) sloped sidewall angle and width difference (compared to the theoretical width of the used GDS file); c) Examples of the disk micro-structure at very low and very high doses, resulting in “bowl” and “pancake” shapes, respectively.

## 4. GRATING CHARACTERIZATION

### A. Measurements

Different gratings have been fabricated with  $0.5 \mu\text{m}$  thick  $\text{Y}_2\text{O}_3:\text{Er}^{3+}$  on  $2 \mu\text{m}$   $\text{SiO}_2$  on Si substrate. Figure 4-a presents SEM images for 3, 4.5, 6 and  $8 \mu\text{m}$  periods. We clearly see that high spatial resolution is obtained with sub-micrometric trenches. Photoluminescence and reflectivity measurements were performed on such gratings. Figure 4-b presents the micro-reflectivity measurements performed with an infrared lamp focused over  $10 \mu\text{m}^2$  on the microstructures. Light was collected through a  $\times 50$  objective of numerical aperture  $\text{NA}=0.42$  and directed to a spectrometer with an IR InGaAs camera used as output detector with 10 ms integration time. In order to resolve the angular distribution, the farfield image is captured in the Fourier space by projecting the back-focal plane of the objective on the entrance slits of the spectrograph. The

corrugation direction in the sample is aligned along the spectrometer slit, so that single-shot image taken by the camera provides directly an angle-resolved reflectivity map [40]. The GMRs are revealed in the reflectivity as Fano resonances in the measured spectrum. The associated modeling (similar to the one discussed in Figure 1) have been added as red dashed lines on the measurements with the adjusted period  $p_{\text{th}}$  indicated on top of the Figure 4-b. We found a very good agreement between the measured and adjusted periods starting from 4 GMRs for the  $3 \mu\text{m}$  period up to 10 for the largest period, as expected. Micro-PL measurements were also performed on the same microstructures with a  $532 \text{ nm}$  wavelength CW laser and the same measurement setup (Figure 4-c). First of all, we observe the expected erbium transition in  $\text{Y}_2\text{O}_3$  poly-crystalline matrix with a maximum emission at  $1.54 \mu\text{m}$  wavelength [41]. Secondly, we observe that the photoluminescence intensity is highly increased at angular positions driven by the GMR dispersions. For instance, the emission is enhanced at two angles ( $\pm 10^\circ$ ) for the  $3 \mu\text{m}$  period, which correspond to the diffracted modes observed by the reflectivity measurement (Figure 4).

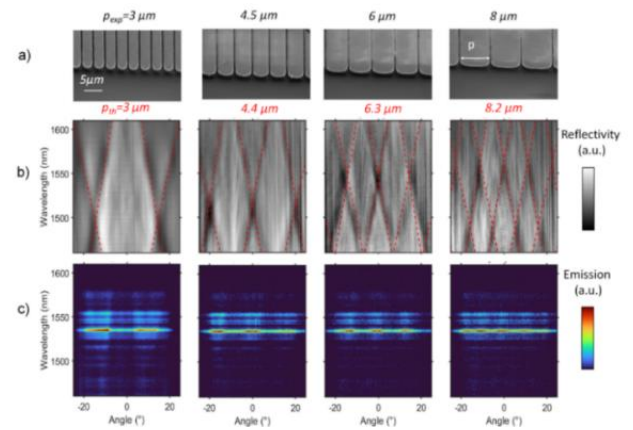


Fig. 4. Diffraction gratings characterization for different periods with a) SEM tilted image; b) reflectivity and c) photoluminescence measurements as a function of the wavelength and the angle.

### B. Photoluminescence enhancement

In order to evaluate quantitatively the luminescence enhancement, the gratings were compared to the unstructured part of the sample. The Figure 5-a presents the luminescence of the bulk layer with the same measurement setup. Since the emitted signal was lower, the integration time used was 10 times higher (i.e 100 ms). We also see a maximum of emission at  $1.54 \mu\text{m}$ . However, no preferential orientation of the emission is observed since rare earth emission is isotropic in bulk materials. Such emission was compared in count/s with the structured layers at  $1.54 \mu\text{m}$  as a function of the emitted angle (Figure 5-c) and at  $-10^\circ$  as function of the wavelength (Figure 5-d). A maximum luminescence enhancement of 15 is reported for the  $3 \mu\text{m}$  period compared to the bulk layer at the maximum of the detected signal (i.e.  $1.54 \mu\text{m}$  and  $-10^\circ$ ). Such improvement results from the extraction enhancement evaluated to be a factor 2 (by comparing the intensity between 0 and  $\pm 10^\circ$ ) and the absorption enhancement evaluated here to be around 7.5 (15 divided by the extraction factor of 2). Indeed, the absorption enhancement of the pump laser is a key factor for luminescence enhancement in diffraction gratings [10]. As it was shown in Figure 1-b, at  $0.54 \mu\text{m}$  wavelength the coupled in-plane modes have an order of around 15 for the  $3 \mu\text{m}$  period while it is closer to 40 for the  $8 \mu\text{m}$  period. According to the diffraction grating theory, the diffraction will be more efficient with lower period since the diffraction occurs with

lower mode giving thus higher absorption. Our maximal enhancement factor (i.e. x15) could thus be further increased using lower periods. Furthermore, the luminescence enhancement is also related to the extraction factor. As indicated by the comparison between the reflection measurement and the photoluminescence (Figure 4-b and c), for the 3  $\mu\text{m}$  period sample, we clearly see that the crossing of both Fano resonances does not fit the maximum of the erbium emission at 1.54  $\mu\text{m}$ . Therefore, the previous enhancement value of 15 at  $\lambda=1.54$   $\mu\text{m}$  could also be further improved by carefully adjusting the Fano resonances at the maximum of the erbium emission using period optimization. Finally, far field measurement was performed on the 6  $\mu\text{m}$  period sample using a spectral filter and a Fourier lens on the beam path. As expected three main modes are observed only along the grating diffraction (Figure 5-b), which confirms that we can control the emission along different directions with such a design.

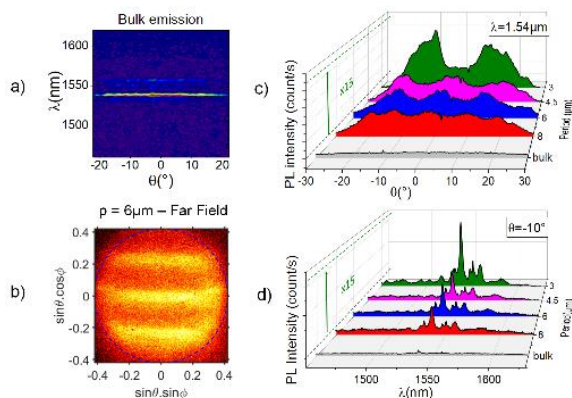


Fig. 5. Diffraction gratings with a) photoluminescence of the unstructured layers as a function of the wavelength and the angle; b) far field photoluminescence measurement in the Fourier plane; Comparison of the emission intensity for the different periods compared to the unstructured layers c) as a function of the angle and d) wavelength

## CONCLUSION

In summary, we have investigated  $\text{Y}_2\text{O}_3:\text{Er}^{3+}$  diffraction gratings made by PLD and lift-off processing. The processing conditions have been first optimized showing that the lithography dose is a key parameter to control the sidewall angle and to reach high-resolution patterning. Diffraction gratings have then been fabricated down to a period of 3  $\mu\text{m}$ . Reflectivity and photoluminescence measurements of such devices show a very good agreement with modeling, with a maximum luminescence enhancement of 15 compared to unstructured layer. Therefore, this work highlights the PLD based lift-off processing to fabricate photonics devices. It opens thus perspectives to the realization of new microstructures for integrated optics without etching, for future applications in free-space communications and integrated quantum optics.

**Acknowledgments.** The authors would like to thank the NanoLyon platform for the cleanroom facilities. Salahedine Toubi, Ylyes Betka for their M1 projects and the ILM for funding.

**Disclosures.** The authors declare no conflicts of interest.

## References

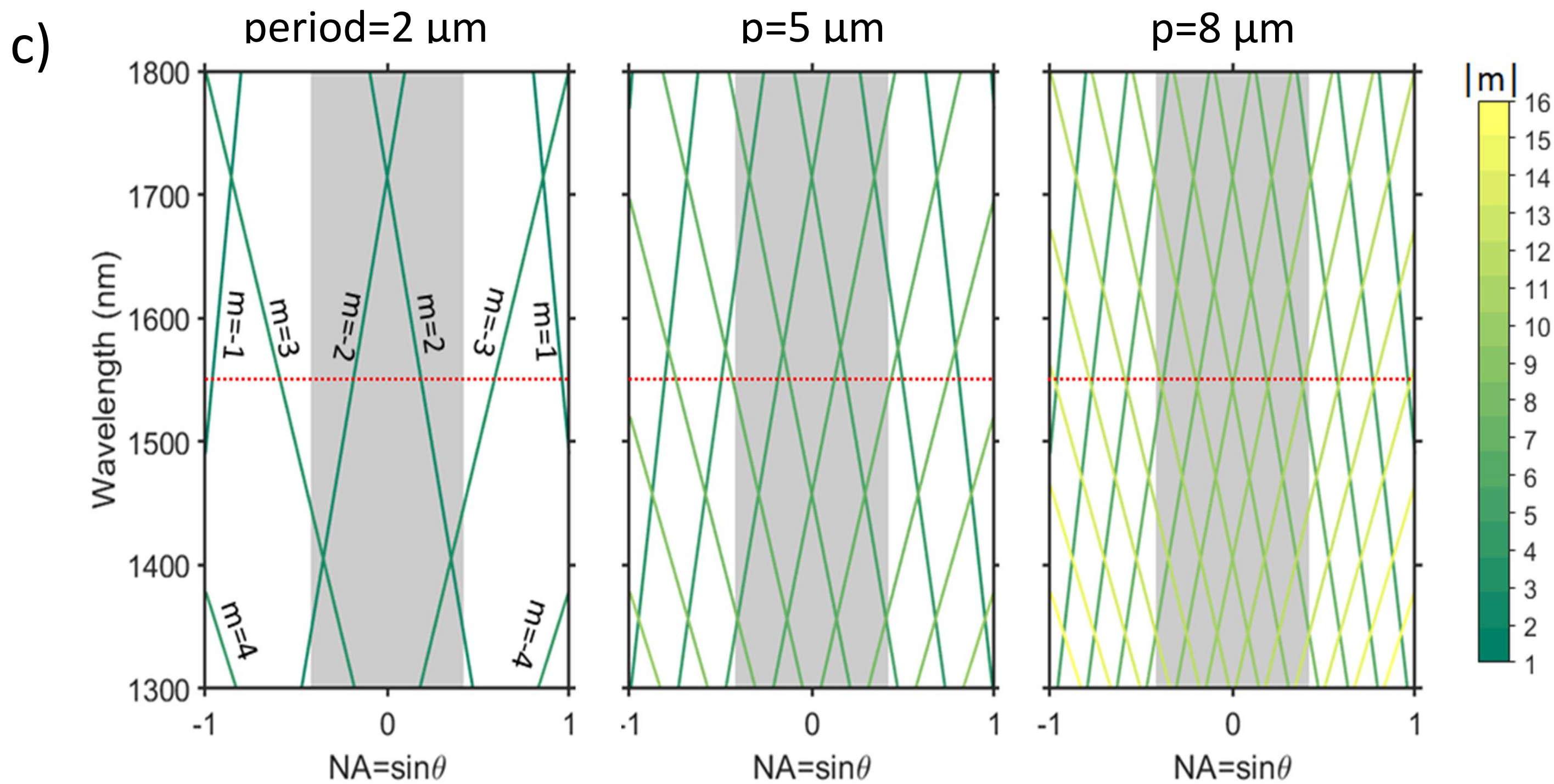
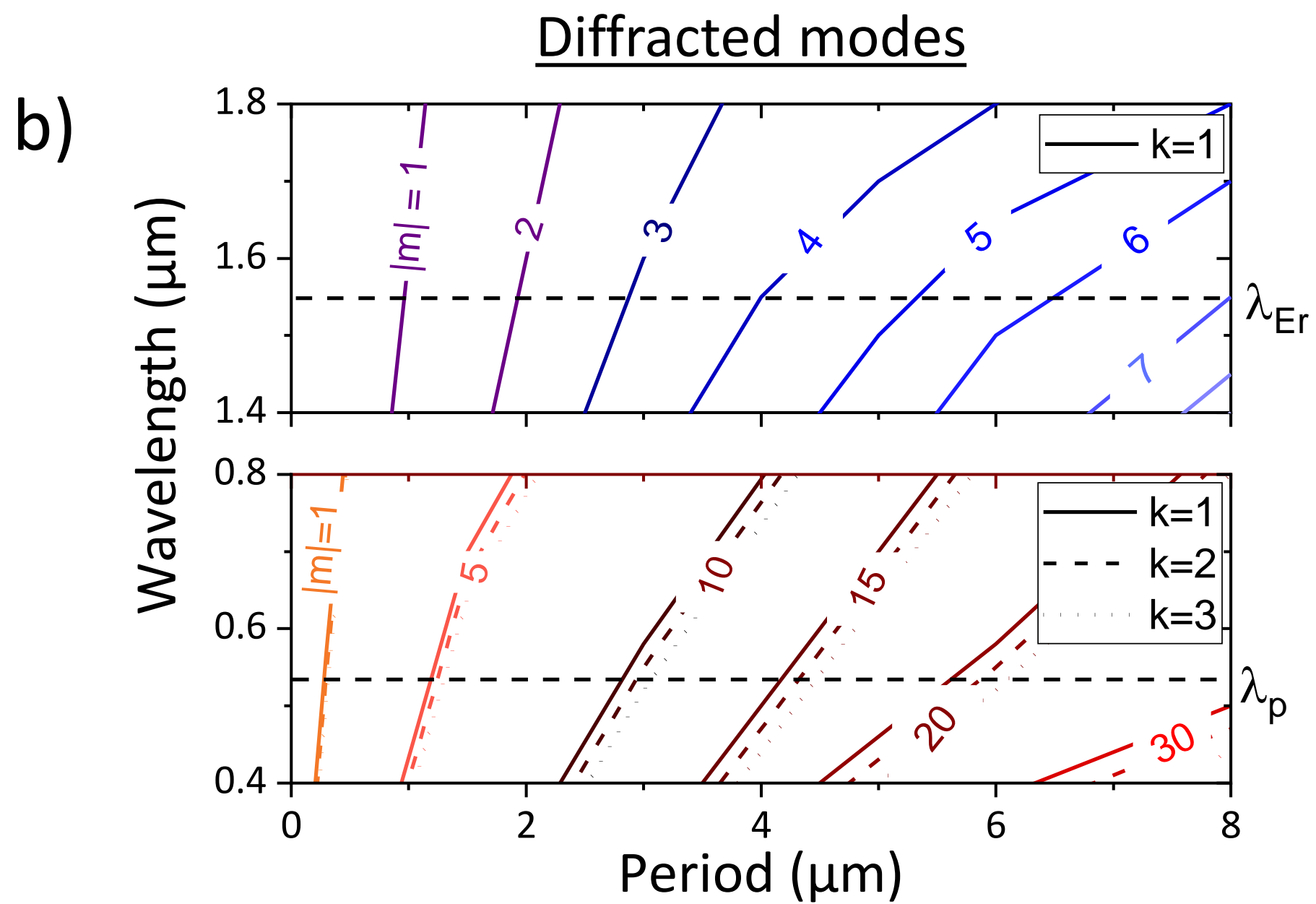
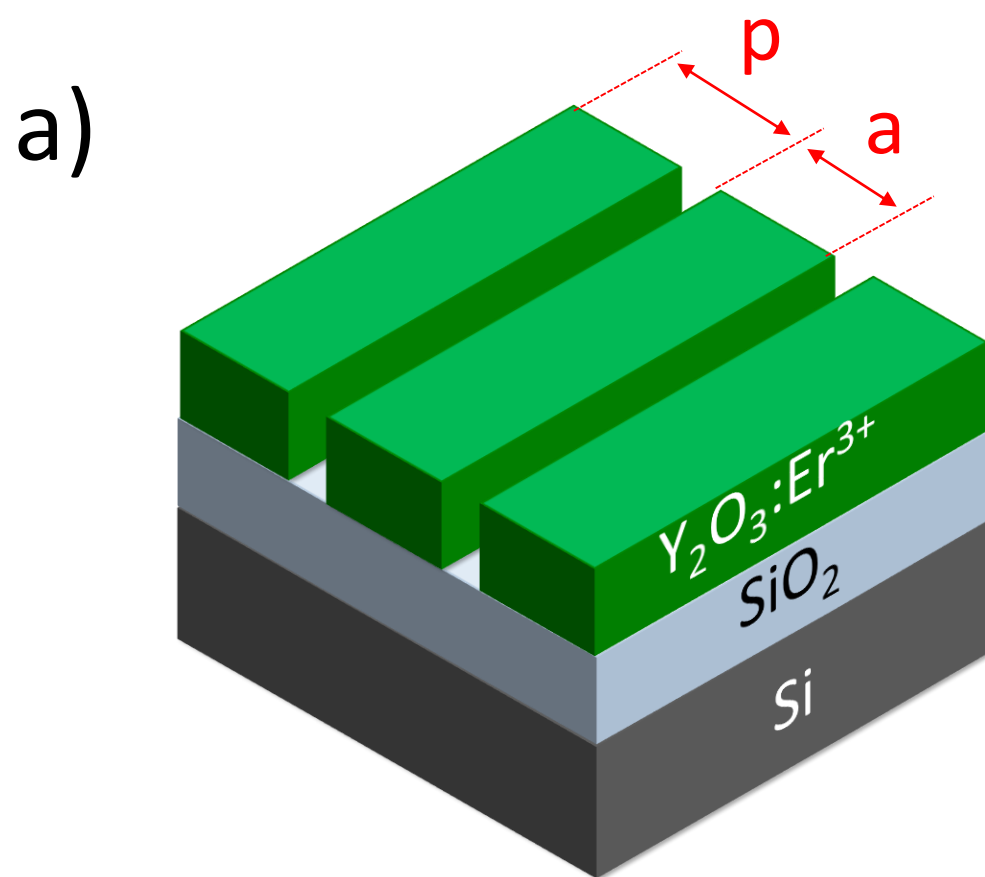
1. L. Megalini, R. Shenoy, K. Rose, J. P. Speck, J. E. Bowers, S. Nakamura, D. A. Cohen, and S. P. DenBaars, *Phys. Status Solidi Appl. Mater. Sci.* **213**, 953 (2016).
2. L. Megalini, R. Shenoy, K. Rose, J. P. Speck, J. E. Bowers, S. Nakamura, D. A. Cohen, S. P. DenBaars, M. Takenaka, K. Morii,

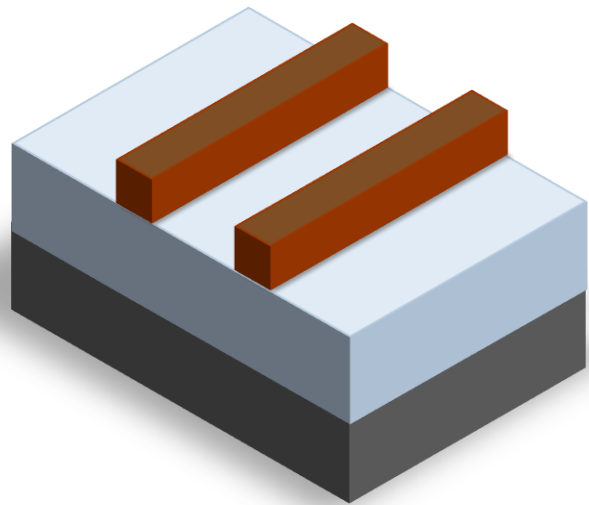
- M. Sugiyama, Y. Nakano, and S. Takagi, *Opt. Express* **20**, 8718 (2012).
3. A. K. Agarwal, *Fiber Integr. Opt.* (1987).
4. K. T. V. Grattan, *Opt. Laser Technol.* (1998).
5. C. Yang, L. Liang, L. Qin, H. Tang, Y. Lei, P. Jia, Y. Chen, Y. Wang, Y. Song, C. Qiu, C. Zheng, H. Zhao, X. Li, D. Li, and L. Wang, *Nanophotonics* (2023).
6. P. Karvinen, T. Nuutinen, J. Rahomäki, O. Hyvärinen, and P. Vahimaa, *Opt. Lett.* **34**, 3208 (2009).
7. X. Xu, H. Kwon, S. Finch, J. Y. Lee, L. Nordin, D. Wasserman, A. Alù, and A. Dodabalapur, *Appl. Phys. Lett.* **118**, (2021).
8. D. T. Vu, H. W. Chiu, R. Nababan, Q. M. Le, S. W. Kuo, L. K. Chau, C. C. Ting, H. C. Kan, and C. C. Hsu, *ACS Photonics* **5**, 3263 (2018).
9. Y. Gong, S. Yerci, R. Li, L. Dal Negro, and J. Vuckovic, *Opt. Express* **17**, 20642 (2009).
10. N. V. Hoang, A. Pereira, H. S. Nguyen, E. Drouard, B. Moine, T. Deschamps, R. Orobtcouk, A. Pillonnet, and C. Seassal, *ACS Photonics* **4**, 1705 (2017).
11. Y. Meng, Y. Chen, L. Lu, Y. Ding, A. Cusano, J. A. Fan, Q. Hu, K. Wang, Z. Xie, Z. Liu, Y. Yang, Q. Liu, M. Gong, Q. Xiao, S. Sun, M. Zhang, X. Yuan, and X. Ni, *Light Sci. Appl.* **10**, 1 (2021).
12. M. Wang, Z. Shang, X. Yan, G. Shi, H. Cao, W. Ma, and T. Jiao, *Opt. Commun.* **481**, 126522 (2021).
13. L. Agazzi, J. D. B. Bradley, M. Dijkstra, F. Ay, G. Roelkens, R. Baets, K. Wörhoff, and M. Pollnau, *Opt. Express* **18**, 27703 (2010).
14. S. Dutta, E. A. Goldschmidt, S. Barik, U. Saha, and E. Waks, *Nano Lett.* **20**, 741 (2020).
15. P. Xing, G. F. R. Chen, X. Zhao, D. K. T. Ng, M. C. Tan, and D. T. H. Tan, *Nat. Commun.* **7**, 1 (2017).
16. Kangwei Xia 1, 2, Fiammetta Sardi 1 7 + Colin Sauerzapf 1 Thomas Kornher, H.-W. Becker, Z. Kis, L. Kovacs, D. Dertli, J. Foglszinger, R. Kolesov, and J. Wrachtrup, *Optica* **9**, (2022).
17. M. Raha, S. Chen, C. M. Phenicie, S. Ourari, A. M. Dibos, and J. D. Thompson, *Nat. Commun.* **11**, 1 (2020).
18. R. W. Eason, T. C. May-Smith, C. Grivas, M. S. B. Darby, D. P. Shepherd, and R. Gazia, *Appl. Surf. Sci.* **255**, 5199 (2009).
19. X. Jiang, D. Pak, A. Nandi, Y. Xuan, and M. Hosseini, *Appl. Phys. Lett.* **115**, 1104 (2019).
20. Purnawirman, J. Sun, T. N. Adam, G. Leake, D. Coolbaugh, J. D. B. Bradley, E. S. Hosseini, and M. R. Watts, *Opt. Lett.* **38**, 1760 (2013).
21. A. Ruiz-Caridad, S. Collin, C. Alonso-Ramos, G. Agnus, S. Guerber, C. Baudot, F. Boeuf, S. Monfray, S. Cremer, V. Vakarín, E. Cassan, G. Marcaud, D. Marris-Morini, P. Lecoeur, L. Vivien, J. M. Ramirez, J. Zhang, E. Duran-Valdeiglesias, C. Lafforge, L. Largeau, T. Maroutian, and S. Matzen, *IEEE J. Quantum Electron.* **56**, 1 (2020).
22. A. Ruskuc, C. J. Wu, J. Rochman, J. Choi, and A. Faraon, *Nature* **602**, 408 (2022).
23. J. G. Bartholomew, J. Rochman, T. Xie, J. M. Kindem, A. Ruskuc, I. Craiciu, M. Lei, and A. Faraon, *Nat. Commun.* **11**, (2020).
24. J. M. Kindem, A. Ruskuc, J. G. Bartholomew, J. Rochman, Y. Q. Huan, and A. Faraon, *Nature* **580**, 201 (2020).
25. J. Rönn, W. Zhang, A. Autere, X. Leroux, L. Pakarinen, C. Alonso-Ramos, A. Säynätjoki, H. Lipsanen, L. Vivien, E. Cassan, and Z. Sun, *Nat. Commun.* **10**, 1 (2019).
26. N. Li, M. Xin, Z. Su, E. S. Magden, N. Singh, J. Notaros, E. Timurdogan, P. Purnawirman, J. D. B. Bradley, and M. R. Watts, *Sci. Rep.* **10**, 1 (2020).
27. T. Zhong and P. Goldner, *Nanophotonics* **8**, 2003 (2019).
28. P. Stevenson, C. M. Phenicie, I. Gray, S. P. Horvath, S. Welinski, A. M. Ferrenti, A. Ferrier, P. Goldner, S. Das, R. Ramesh, R. J. Cava, N. P. de Leon, and J. D. Thompson, *Phys. Rev. B* **105**, (2022).
29. P. Siyushev, K. Xia, R. Reuter, M. Jamali, N. Zhao, N. Yang, C. Duan, N. Kukharchyk, A. D. Wieck, R. Kolesov, and J. Wrachtrup, *Nat. Commun.* **5**, 1 (2014).
30. N. Li, E. S. Magden, Z. Su, N. Singh, A. Ruocco, M. Xin, M. Byrd, P. T. Callahan, J. D. B. Bradley, D. Vermeulen, and M. R. Watts, *Opt. Express* **26**, 4560 (2018).

31. R. L. Cone, C. W. Thiel, Y. Sun, T. Böttger, and R. M. Macfarlane, *Adv. Photonics Quantum Comput. Mem. Commun.* V **8272**, 82720E (2012).
32. D. Berkoh and S. Kulkarni, *IEEE Trans. Semicond. Manuf.* **32**, 513 (2019).
33. E. Tolstosheeva, E. Barborini, E. M. Meyer, M. Shafi, S. Vinati, and W. Lang, *J. Micromechanics Microengineering* **24**, (2014).
34. C. M. Quintana, A. Megrant, Z. Chen, A. Dunsworth, B. Chiaro, R. Barends, B. Campbell, Y. Chen, E. Jeffrey, J. Kelly, J. Y. Mutus, P. J. J. O. Malley, C. Neill, P. Roushan, D. Sank, A. Vainsencher, J. Wenner, T. C. White, A. N. Cleland, and J. M. Martinis, *Appl. Phys. Lett* **105**, 1 (2014).
35. H. Fujioka, *Handb. Cryst. Growth Thin Film. Ep.* **8**, 365 (2015).
36. A. Gassenq, E. Cleyet-Merle, H. Sahib, B. Baguenard, A. Belarouci, R. Orobtschouk, F. Lerouge, S. Guy, and A. Pereira, *Opt. Express* **29**, 7321 (2021).
37. Y. Nigara, *Jpn. J. Appl. Phys.* (1968).
38. I. H. Malitson, *J. Opt. Soc. Am.* **55**, 1205 (1965).
39. G. Marin, (2015).
40. R. Wagner, L. Heerklotz, N. Kortenbruck, and F. Cichos, *Appl. Phys. Lett.* (2012).
41. A. N. Georgobiani, A. N. Gruzintsev, A. C. Barthou, and P. Benalloul, *Inorg. Mater.* **40**, 963 (2004).

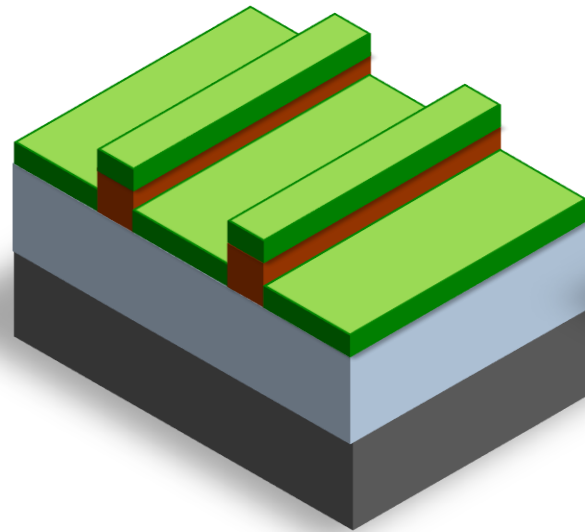
## References list that contains titles

- (1) Megalini, L.; Shenoy, R.; Rose, K.; Speck, J. P.; Bowers, J. E.; Nakamura, S.; Cohen, D. A.; DenBaars, S. P. Estimation of Roughness-Induced Scattering Losses in III-Nitride Laser Diodes with a Photoelectrochemically Etched Current Aperture. *Phys. Status Solidi Appl. Mater. Sci.* 2016, 213 (4), 953–957. <https://doi.org/10.1002/pssa.201532540>
- (2) Megalini, L.; Shenoy, R.; Rose, K.; Speck, J. P.; Bowers, J. E.; Nakamura, S.; Cohen, D. A.; DenBaars, S. P.; Takenaka, M.; Morii, K.; Sugiyama, M.; Nakano, Y.; Takagi, S. Dark Current Reduction of Ge Photodetector by GeO<sub>2</sub> Surface Passivation and Gas-Phase Doping. *Opt. Express* 2012, 20 (8), 8718. <https://doi.org/10.1364/oe.20.008718>
- (3) Agarwal, A. K. Review of Optical Fiber Couplers. *Fiber Integr. Opt.* 1987. <https://doi.org/10.1080/01468038708219344>
- (4) Grattan, K. T. V. Handbook of Distributed Feedback Laser Diodes. *Opt. Laser Technol.* 1998. [https://doi.org/10.1016/s0030-3992\(98\)00002-4](https://doi.org/10.1016/s0030-3992(98)00002-4)
- (5) Yang, C.; Liang, L.; Qin, L.; Tang, H.; Lei, Y.; Jia, P.; Chen, Y.; Wang, Y.; Song, Y.; Qiu, C.; Zheng, C.; Zhao, H.; Li, X.; Li, D.; Wang, L. Advances in Silicon-Based, Integrated Tunable Semiconductor Lasers. *Nanophotonics*. 2023. <https://doi.org/10.1515/nanoph-2022-0699>
- (6) Karvinen, P.; Nuutinen, T.; Rahomäki, J.; Hyvärinen, O.; Vahimaa, P. Strong Fluorescence-Signal Gain with Single-Excitation-Enhancing and Emission-Directing Nanostructured Diffraction Grating. *Opt. Lett.* 2009, 34 (20), 3208. <https://doi.org/10.1364/ol.34.003208>
- (7) Xu, X.; Kwon, H.; Finch, S.; Lee, J. Y.; Nordin, L.; Wasserman, D.; Alù, A.; Dodabalapur, A. Reflecting Metagrating-Enhanced Thin-Film Organic Light Emitting Devices. *Appl. Phys. Lett.* 2021, 118 (5). <https://doi.org/10.1063/5.0034573>
- (8) Vu, D. T.; Chiu, H. W.; Nababan, R.; Le, Q. M.; Kuo, S. W.; Chau, L. K.; Ting, C. C.; Kan, H. C.; Hsu, C. C. Enhancing Upconversion Luminescence Emission of Rare Earth Nanophosphors in Aqueous Solution with Thousands Fold Enhancement Factor by Low Refractive Index Resonant Waveguide Grating. *ACS Photonics* 2018, 5 (8), 3263–3271. <https://doi.org/10.1021/acsp Photonics.8b00494>
- (9) Gong, Y.; Yerci, S.; Li, R.; Dal Negro, L.; Vuckovic, J. Enhanced Light Emission from Erbium Doped Silicon Nitride in Plasmonic Metal-Insulator-Metal Structures. *Opt. Express* 2009, 17 (23), 20642. <https://doi.org/10.1364/oe.17.020642>
- (10) Hoang, N. V.; Pereira, A.; Nguyen, H. S.; Drouard, E.; Moine, B.; Deschamps, T.; Orobtcouk, R.; Pillonnet, A.; Seassal, C. Giant Enhancement of Luminescence Down-Shifting by a Doubly Resonant Rare-Earth-Doped Photonic Metastructure. *ACS Photonics* 2017, 4 (7), 1705–1712. <https://doi.org/10.1021/acsp Photonics.7b00177>
- (11) Meng, Y.; Chen, Y.; Lu, L.; Ding, Y.; Cusano, A.; Fan, J. A.; Hu, Q.; Wang, K.; Xie, Z.; Liu, Z.; Yang, Y.; Liu, Q.; Gong, M.; Xiao, Q.; Sun, S.; Zhang, M.; Yuan, X.; Ni, X. Optical Meta-Waveguides for Integrated Photonics and Beyond. *Light Sci. Appl.* 2021, 10 (1), 1–44. <https://doi.org/10.1038/s41377-021-00655-x>
- (12) Wang, M.; Shang, Z.; Yan, X.; Shi, G.; Cao, H.; Ma, W.; Jiao, T. Enhance Fluorescence Study of Grating Structure Based on Three Kinds of Optical Disks. *Opt. Commun.* 2021, 481 (September 2020), 126522. <https://doi.org/10.1016/j.optcom.2020.126522>
- (13) Agazzi, L.; Bradley, J. D. B.; Dijkstra, M.; Ay, F.; Roelkens, G.; Baets, R.; Wörhoff, K.; Pollnau, M. Monolithic Integration of Erbium-Doped Amplifiers with Silicon-on-Insulator Waveguides. *Opt. Express* 2010, 18 (26), 27703. <https://doi.org/10.1364/oe.18.027703>
- (14) Dutta, S.; Goldschmidt, E. A.; Barik, S.; Saha, U.; Waks, E. Integrated Photonic Platform for Rare-Earth Ions in Thin Film Lithium Niobate. *Nano Lett.* 2020, 20 (1), 741–747. <https://doi.org/10.1021/acs.nanolett.9b04679>
- (15) Xing, P.; Chen, G. F. R.; Zhao, X.; Ng, D. K. T.; Tan, M. C.; Tan, D. T. H. Silicon Rich Nitride Ring Resonators for Rare-Earth Doped Telecommunications-Band Amplifiers Pumped at the O-Band. *Nat. Commun.* 2017, 7 (1), 1–9. <https://doi.org/10.1038/s41467-019-08369-w>
- (16) 1, 6 Kangwei Xia; 1 Thomas Kornher; 2 Fiammetta Sardi 1 7 † Colin Sauerzapf; Becker, H.-W.; Kis, Z.; Kovacs, L.; Dertli, D.; Foglszinger, J.; Kolesov, R.; Wrachtrup, J. Tunable Microcavities Coupled to Rare-Earth Quantum Emitters. *Optica* 2022, 9 (4). <https://doi.org/10.1364/OPTICA.453527>
- (17) Raha, M.; Chen, S.; Phenicie, C. M.; Ourari, S.; Dibos, A. M.; Thompson, J. D. Optical Quantum Nondemolition Measurement of a Single Rare Earth Ion Qubit. *Nat. Commun.* 2020, 11 (1), 1–6. <https://doi.org/10.1038/s41467-020-15138-7>
- (18) Eason, R. W.; May-Smith, T. C.; Grivas, C.; Darby, M. S. B.; Shepherd, D. P.; Gazia, R. Current State-of-the-Art of Pulsed Laser Deposition of Optical Waveguide Structures: Existing Capabilities and Future Trends. *Appl. Surf. Sci.* 2009, 255 (10), 5199–5205. <https://doi.org/10.1016/j.apsusc.2008.07.133>
- (19) Jiang, X.; Pak, D.; Nandi, A.; Xuan, Y.; Hosseini, M. Rare Earth-Implanted Lithium Niobate: Properties and on-Chip Integration. *Appl. Phys. Lett.* 2019, 115 (7), 1104. <https://doi.org/10.1063/1.5098316>
- (20) Purnawirman; Sun, J.; Adam, T. N.; Leake, G.; Coolbaugh, D.; Bradley, J. D. B.; Hosseini, E. S.; Watts, M. R. C- and L-Band Erbium-Doped Waveguide Lasers with Wafer-Scale Silicon Nitride Cavities. *Opt. Lett.* 2013, 38 (11), 1760. <https://doi.org/10.1364/ol.38.001760>
- (21) Ruiz-Cardad, A.; Collin, S.; Alonso-Ramos, C.; Agnès, G.; Guerber, S.; Baudot, C.; Boeuf, F.; Monfray, S.; Cremer, S.; Vakarin, V.; Cassan, E.; Marcaud, G.; Marris-Morini, D.; Lecoeur, P.; Vivien, L.; Ramirez, J. M.; Zhang, J.; Duran-Valdeiglesias, E.; Lafforge, C.; Largeau, L.; Maroutian, T.; Matzen, S. Erbium-Doped Yttria-Stabilized Zirconia Thin Layers for Photonic Applications. *IEEE J. Quantum Electron.* 2020, 56 (2), 1–6. <https://doi.org/10.1109/JQE.2019.2955943>
- (22) Ruskuc, A.; Wu, C. J.; Rochman, J.; Choi, J.; Faraon, A. Nuclear Spin-Wave Quantum Register for a Solid-State Qubit. *Nature* 2022, 602 (7897), 408–413. <https://doi.org/10.1038/s41586-021-04293-6>
- (23) Bartholomew, J. G.; Rochman, J.; Xie, T.; Kindem, J. M.; Ruskuc, A.; Craiciu, I.; Lei, M.; Faraon, A. On-Chip Coherent Microwave-to-Optical Transduction Mediated by Ytterbium in YVO<sub>4</sub>. *Nat. Commun.* 2020, 11 (1). <https://doi.org/10.1038/s41467-020-16996-x>
- (24) Kindem, J. M.; Ruskuc, A.; Bartholomew, J. G.; Rochman, J.; Huan, Y. Q.; Faraon, A. Control and Single-Shot Readout of an Ion Embedded in a Nanophotonic Cavity. *Nature* 2020, 580 (7802), 201–204. <https://doi.org/10.1038/s41586-020-2160-9>
- (25) Rönn, J.; Zhang, W.; Autere, A.; Leroux, X.; Pakarinen, L.; Alonso-Ramos, C.; Säynätjoki, A.; Lipsanen, H.; Vivien, L.; Cassan, E.; Sun, Z. Ultra-High on-Chip Optical Gain in Erbium-Based Hybrid Slot Waveguides. *Nat. Commun.* 2019, 10 (1), 1–9. <https://doi.org/10.1038/s41467-019-08369-w>
- (26) Li, N.; Xin, M.; Su, Z.; Magden, E. S.; Singh, N.; Notaros, J.; Timurdogan, E.; Purnawirman, P.; Bradley, J. D. B.; Watts, M. R. A Silicon Photonic Data Link with a Monolithic Erbium-Doped Laser. *Sci. Rep.* 2020, 10 (1), 1–9. <https://doi.org/10.1038/s41598-020-57928-5>
- (27) Zhong, T.; Goldner, P. Emerging Rare-Earth Doped Material Platforms for Quantum Nanophotonics. *Nanophotonics* 2019, 8 (11), 2003–2015. <https://doi.org/10.1515/nanoph-2019-0185>
- (28) Stevenson, P.; Phenicie, C. M.; Gray, I.; Horvath, S. P.; Welinski, S.; Ferrenti, A. M.; Ferrier, A.; Goldner, P.; Das, S.; Ramesh, R.; Cava, R. J.; de Leon, N. P.; Thompson, J. D. Erbium-Implanted Materials for Quantum Communication Applications. *Phys. Rev. B* 2022, 105 (22). <https://doi.org/10.1103/physrevb.105.224106>
- (29) Siyushev, P.; Xia, K.; Reuter, R.; Jamali, M.; Zhao, N.; Yang, N.; Duan, C.; Kukharchyk, N.; Wieck, A. D.; Kolesov, R.; Wrachtrup, J. Coherent Properties of Single Rare-Earth Spin Qubits. *Nat. Commun.* 2014, 5 (May), 1–6. <https://doi.org/10.1038/ncomms4895>
- (30) Li, N.; Magden, E. S.; Su, Z.; Singh, N.; Ruocco, A.; Xin, M.; Byrd, M.; Callahan, P. T.; Bradley, J. D. B.; Vermeulen, D.; Watts, M. R. Broadband 2-Mm Emission on Silicon Chips: Monolithically Integrated Holmium Lasers. *Opt. Express* 2018, 26 (3), 4560–4566. <https://doi.org/https://doi.org/10.1364/OE.26.002220>
- (31) Cone, R. L.; Thiel, C. W.; Sun, Y.; Böttger, T.; Macfarlane, R. M. Rare-Earth-Doped Materials with Application to Optical Signal Processing, Quantum Information Science, and Medical Imaging Technology. *Adv. Photonics Quantum Comput. Mem. Commun.* V 2012, 8272, 82720E. <https://doi.org/10.1117/12.909154>
- (32) Berkoh, D.; Kulkarni, S. Challenges in Lift-off Process Using CAMP Negative Photoresist in III-V IC Fabrication. *IEEE Trans. Semicond. Manuf.* 2019, 32 (4), 513–517. <https://doi.org/10.1109/TSM.2019.2944133>
- (33) Tolstosheeva, E.; Barborini, E.; Meyer, E. M.; Shafi, M.; Vinati, S.; Lang, W. Micropatterning of Nanoparticle Films by Bilayer Lift-Off. *J. Micromechanics Microengineering* 2014, 24 (1). <https://doi.org/10.1088/0960-1317/24/1/015001>
- (34) Quintana, C. M.; Migrant, A.; Chen, Z.; Dunsforth, A.; Chiaro, B.; Barends, R.; Campbell, B.; Chen, Y.; Jeffrey, E.; Kelly, J.; Mutus, J. Y.; Malley, P. J. J. O.; Neill, C.; Roushan, P.; Sank, D.; Vainsencher, A.; Wenner, J.; White, T. C.; Cleland, A. N.; Martinis, J. M. Characterization and Reduction of Microfabrication-Induced Decoherence in Superconducting Quantum Circuits. *Appl. Phys. Lett.* 2014, 105 (062601), 1–6. <https://doi.org/10.1063/1.4893297>
- (35) Fujioka, H. Pulsed Laser Deposition (PLD). *Handb. Cryst. Growth Thin Film. Ep.* 2015, 8, 365–397. <https://doi.org/10.1016/B978-0-444-63304-0.00008-1>
- (36) Gassenq, A.; Cleyet-Merle, E.; Sahib, H.; Bagueunard, B.; Belarouci, A.; Orobtcouk, R.; Lerouge, F.; Guy, S.; Pereira, A. Rare-Earth Doped Micro-Emitters Made by Lift-off Processing in Pulsed Laser Deposited Layers on Si Substrate. *Opt. Express* 2021, 29 (5), 7321. <https://doi.org/10.1364/oe.416450>
- (37) Nigara, Y. Measurement of the Optical Constants of Yttrium Oxide. *Jpn. J. Appl. Phys.* 1968. <https://doi.org/10.1143/jjap.7.404>
- (38) Malitson, I. H. Interspecimen Comparison of the Refractive Index of Fused Silica. *J. Opt. Soc. Am.* 1965, 55, 1205. <https://doi.org/10.1364/josa.55.001205>
- (39) Marin, G. Inclined Lithography and Photoresist Optimization for Fabrication of 3D Mesh Structures School of Electrical Engineering, 2015. <https://doi.org/10.13140/RG.2.1.1526.2164>
- (40) Wagner, R.; Heerklotz, L.; Kortenbruck, N.; Cichos, F. Back Focal Plane Imaging Spectroscopy of Photonic Crystals. *Appl. Phys. Lett.* 2012. <https://doi.org/10.1063/1.4746251>
- (41) Georgobiani, A. N.; Grizintsev, A. N.; C. Barthou, A.; Benalloul, P. Infrared Luminescence of Y<sub>2</sub>O<sub>3</sub>:Er<sup>3+</sup> and Y<sub>2</sub>O<sub>3</sub>:Er<sup>3+</sup>. *Inorg. Mater.* 2004, 40 (8), 963–968. <https://doi.org/0020-1685/04/4008-0840>

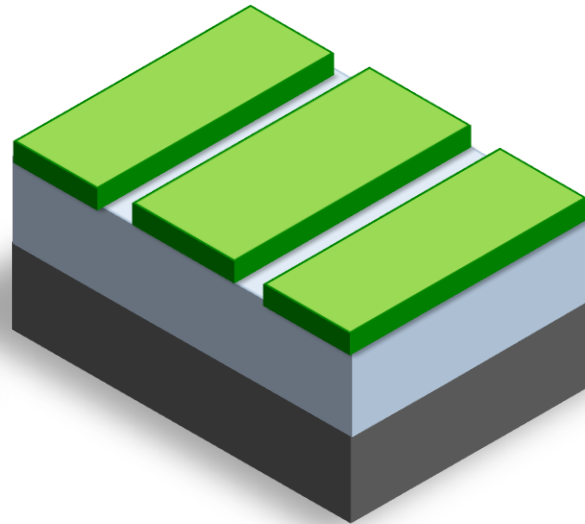




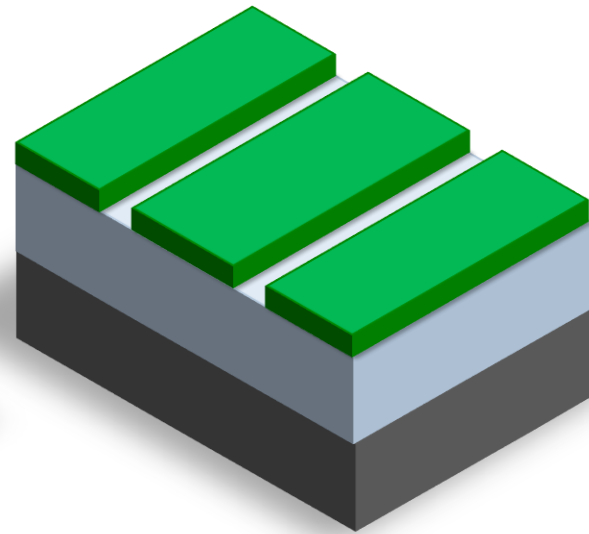
*a)*



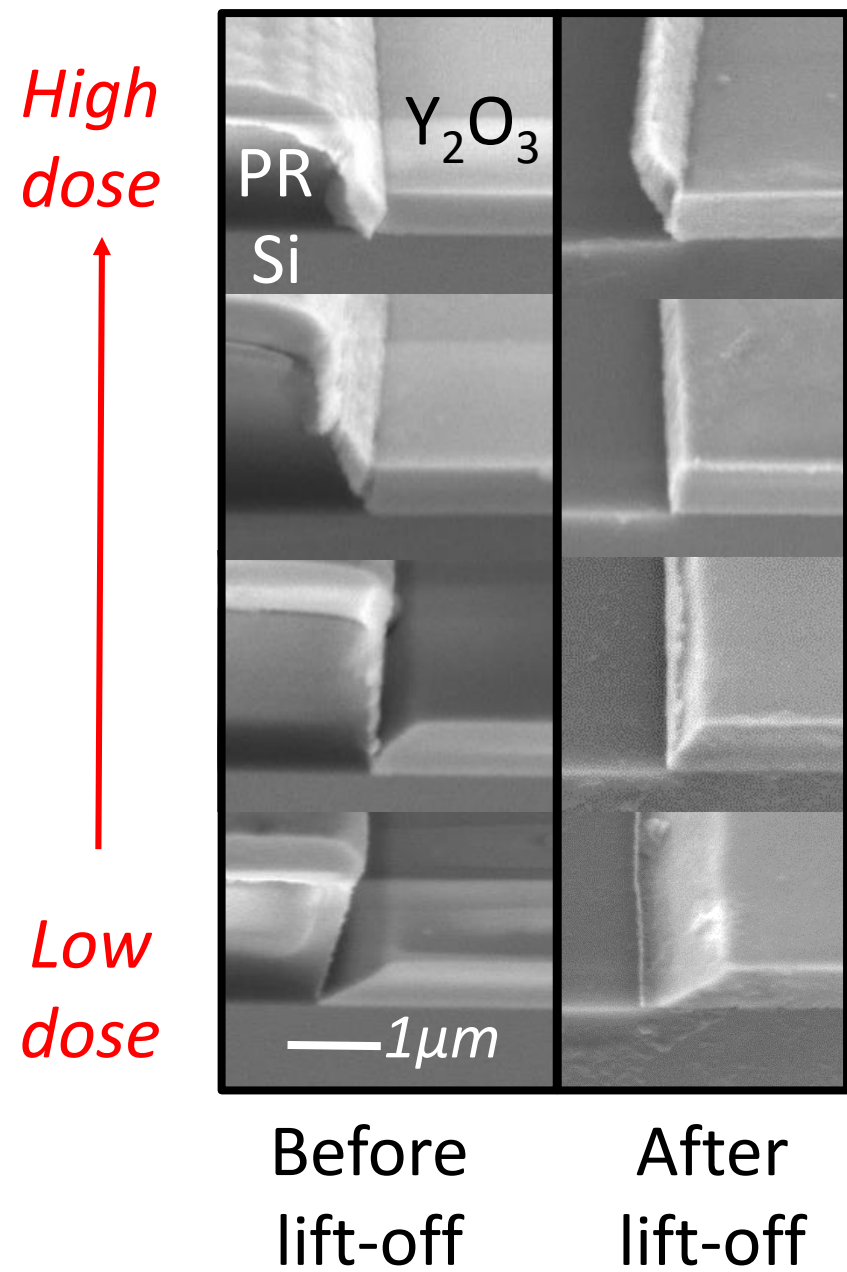
*b)*



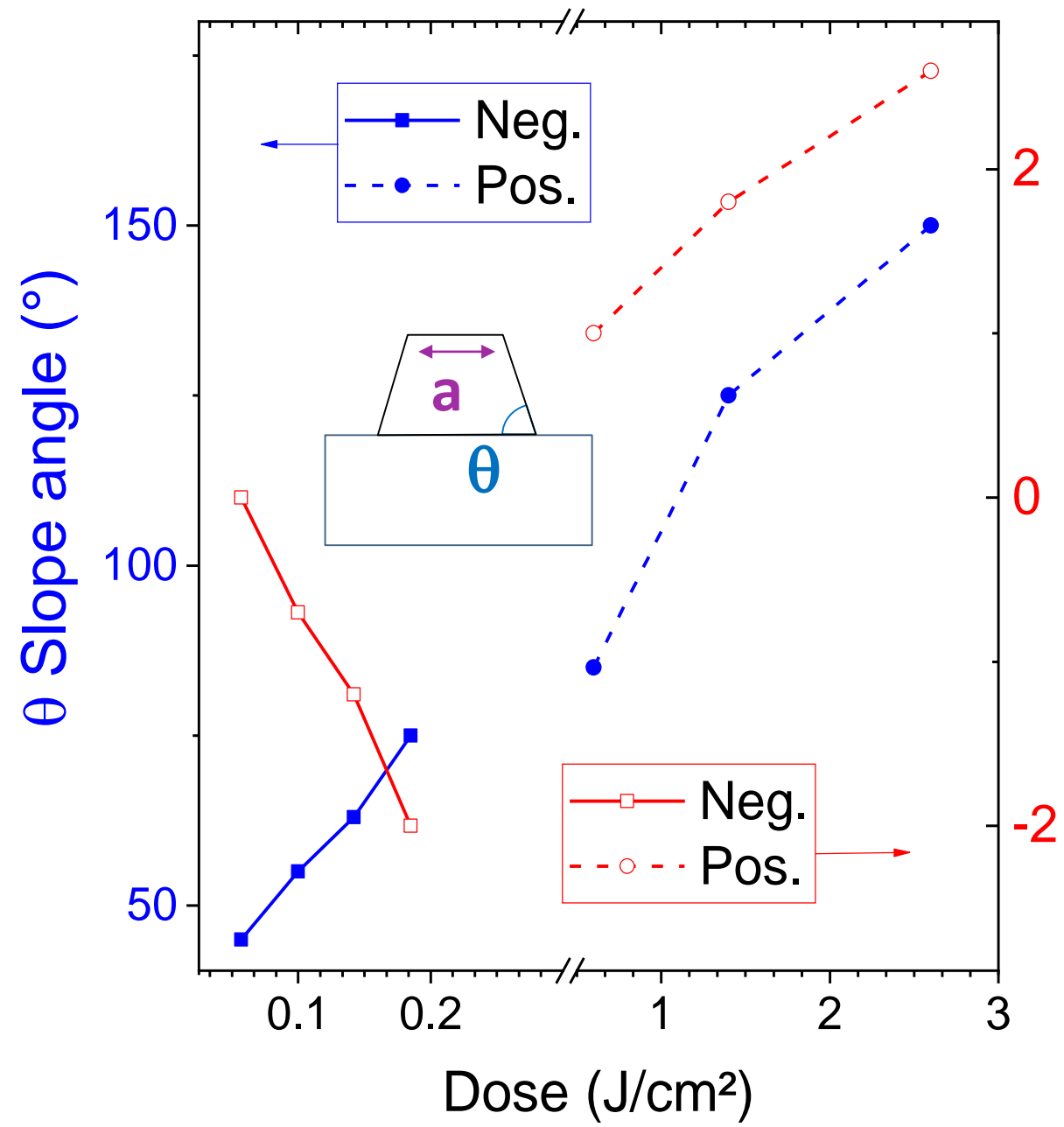
*c)*



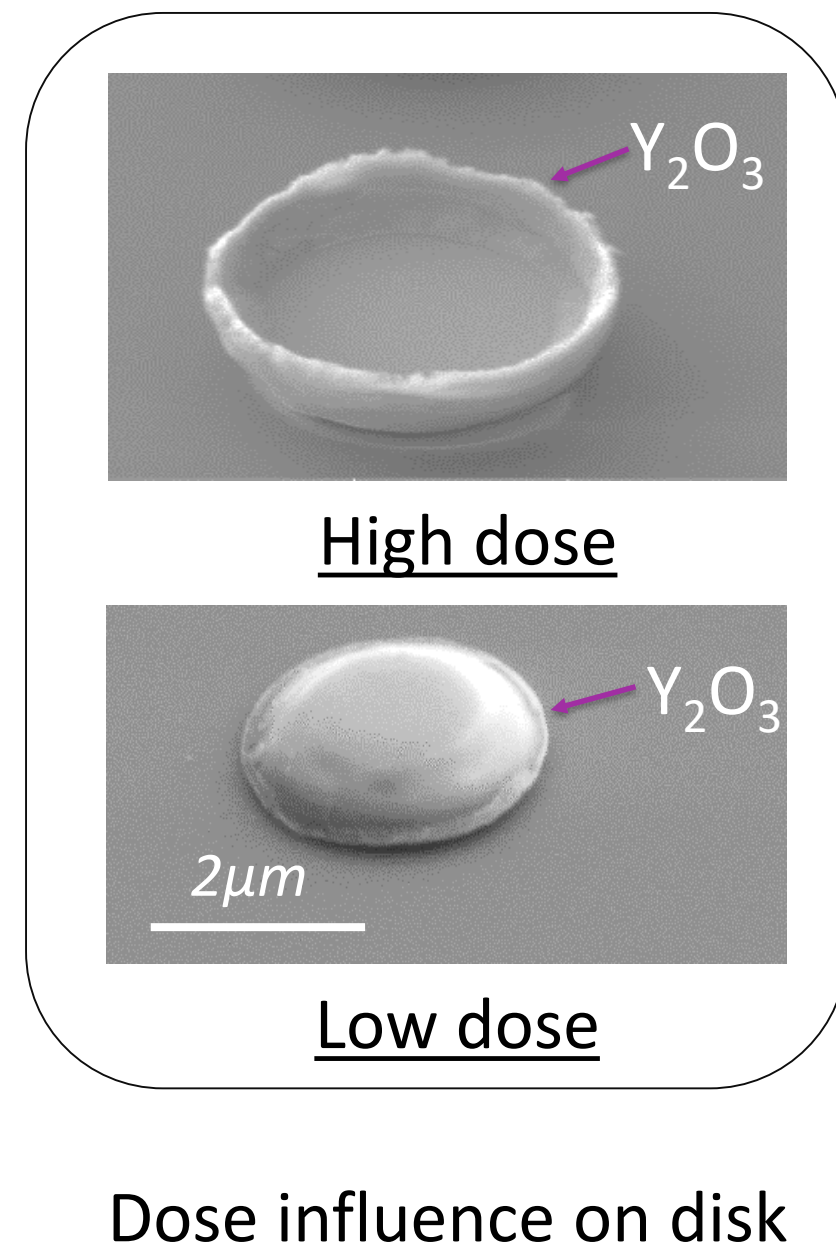
*d)*



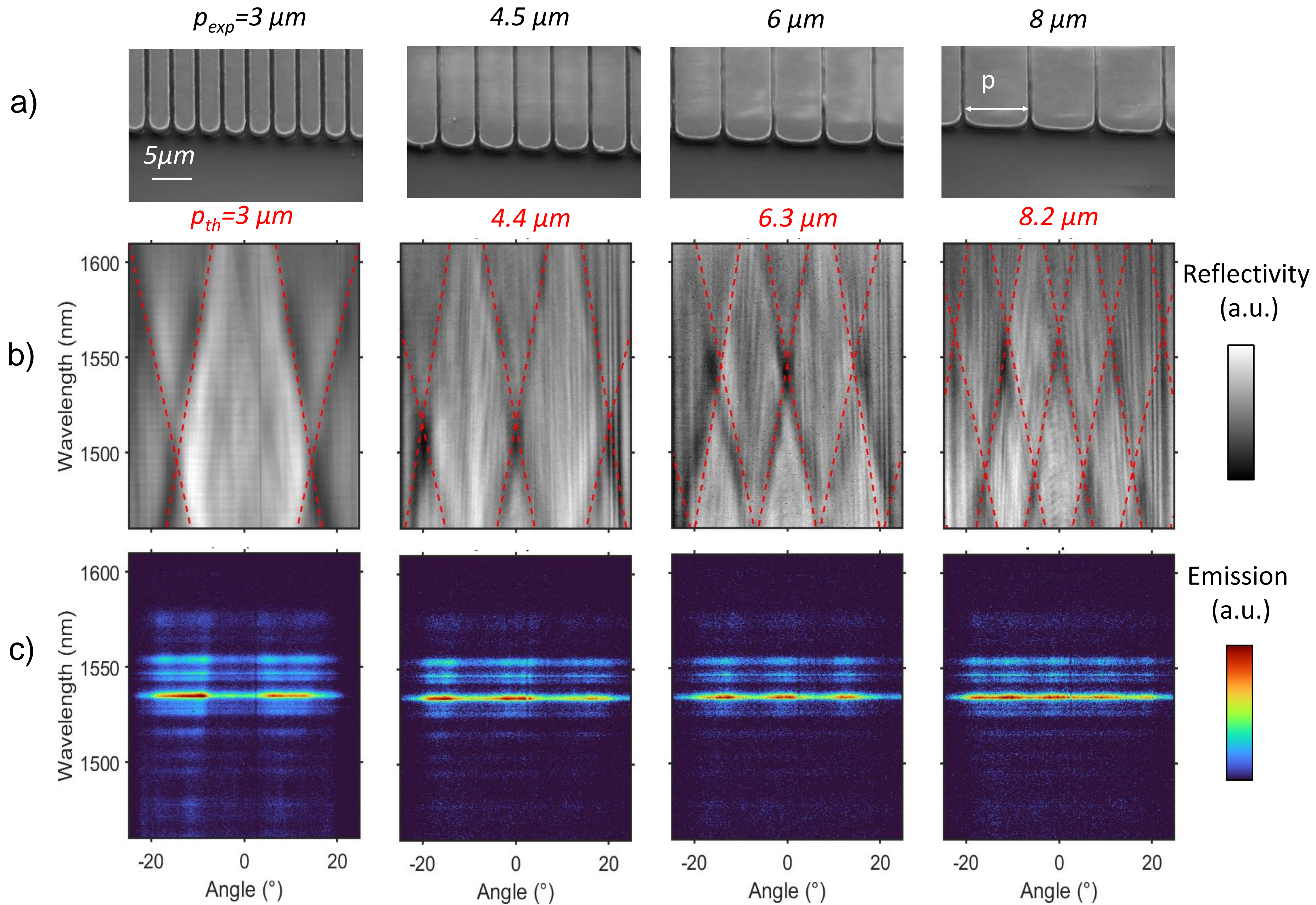
a)



b)

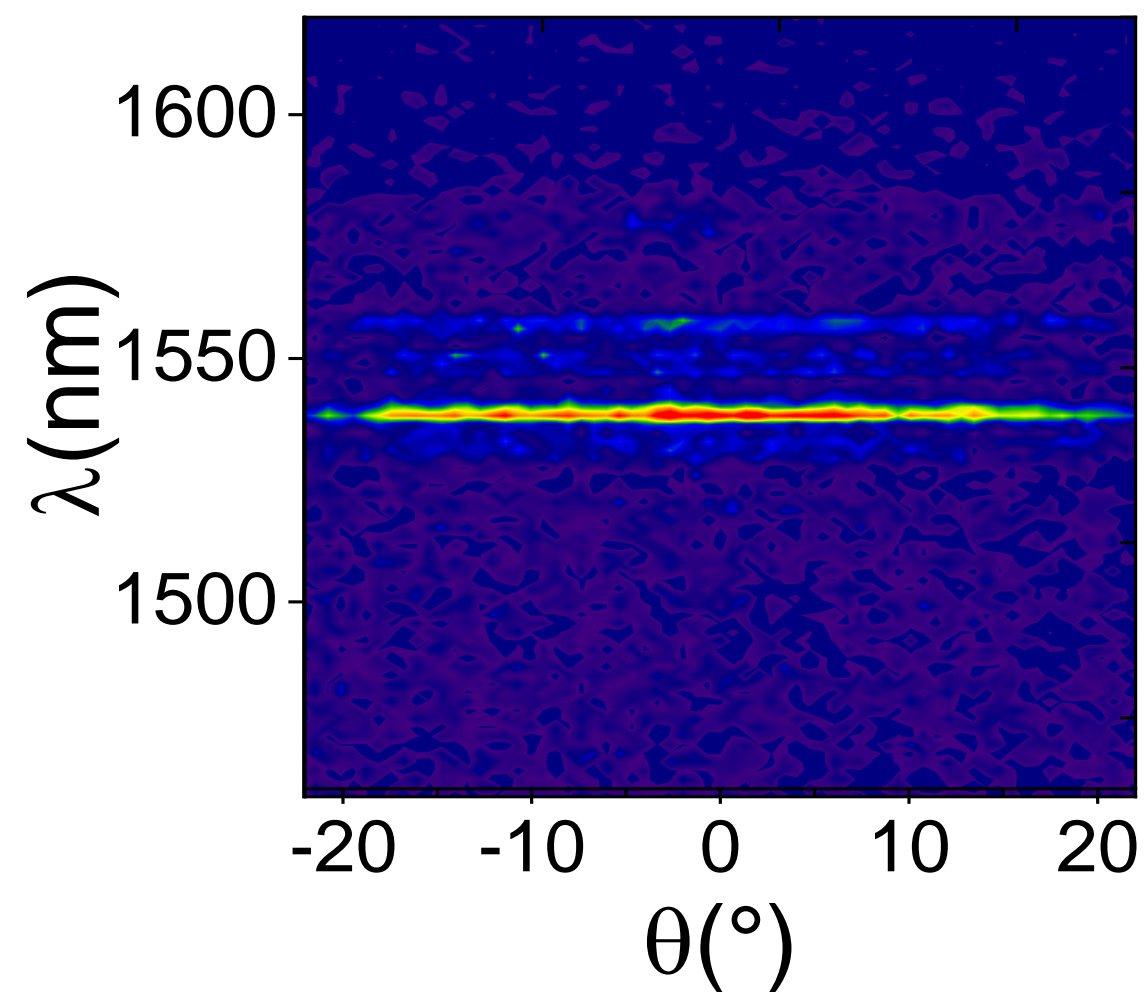


c)

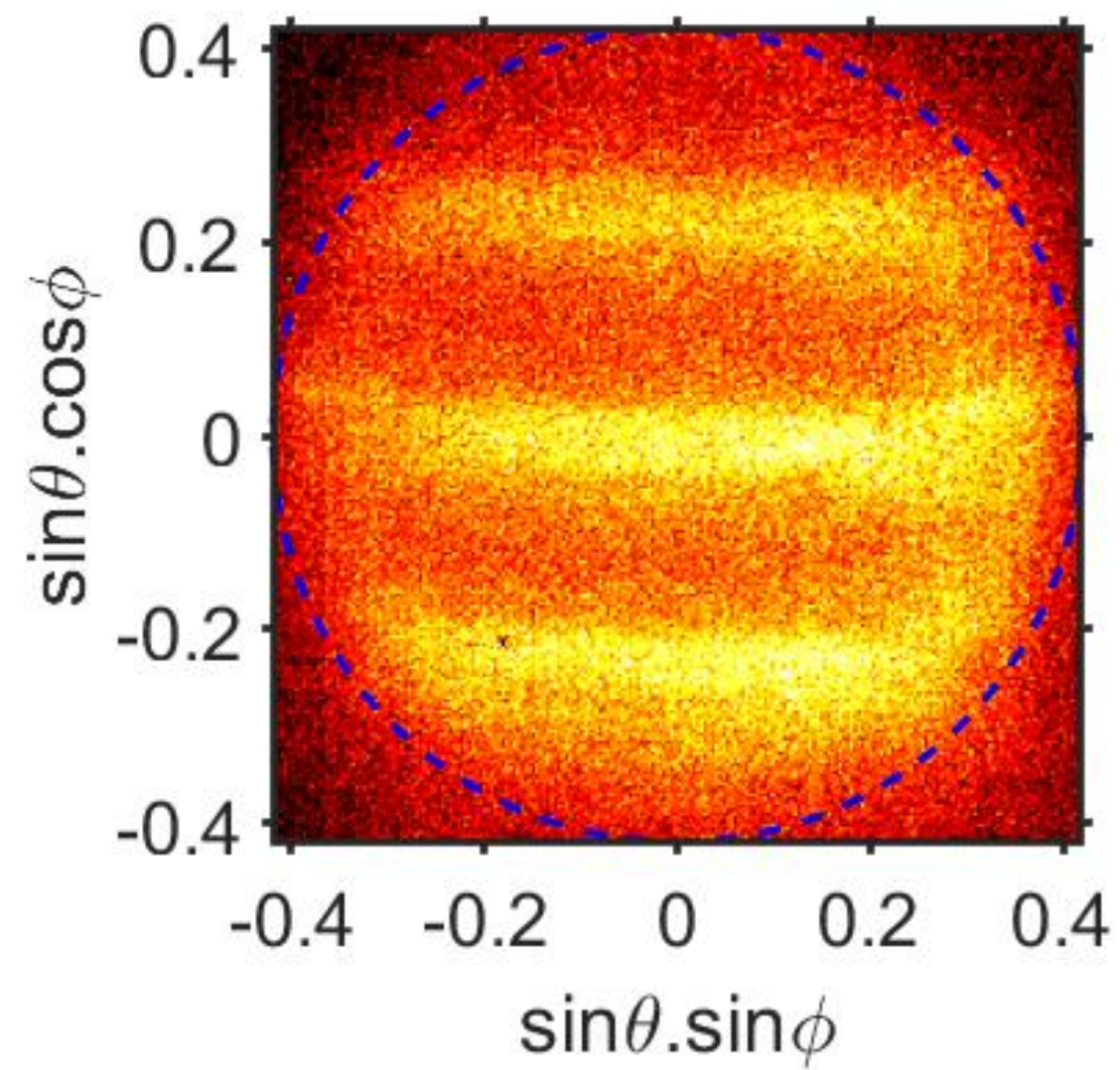


Bulk emission

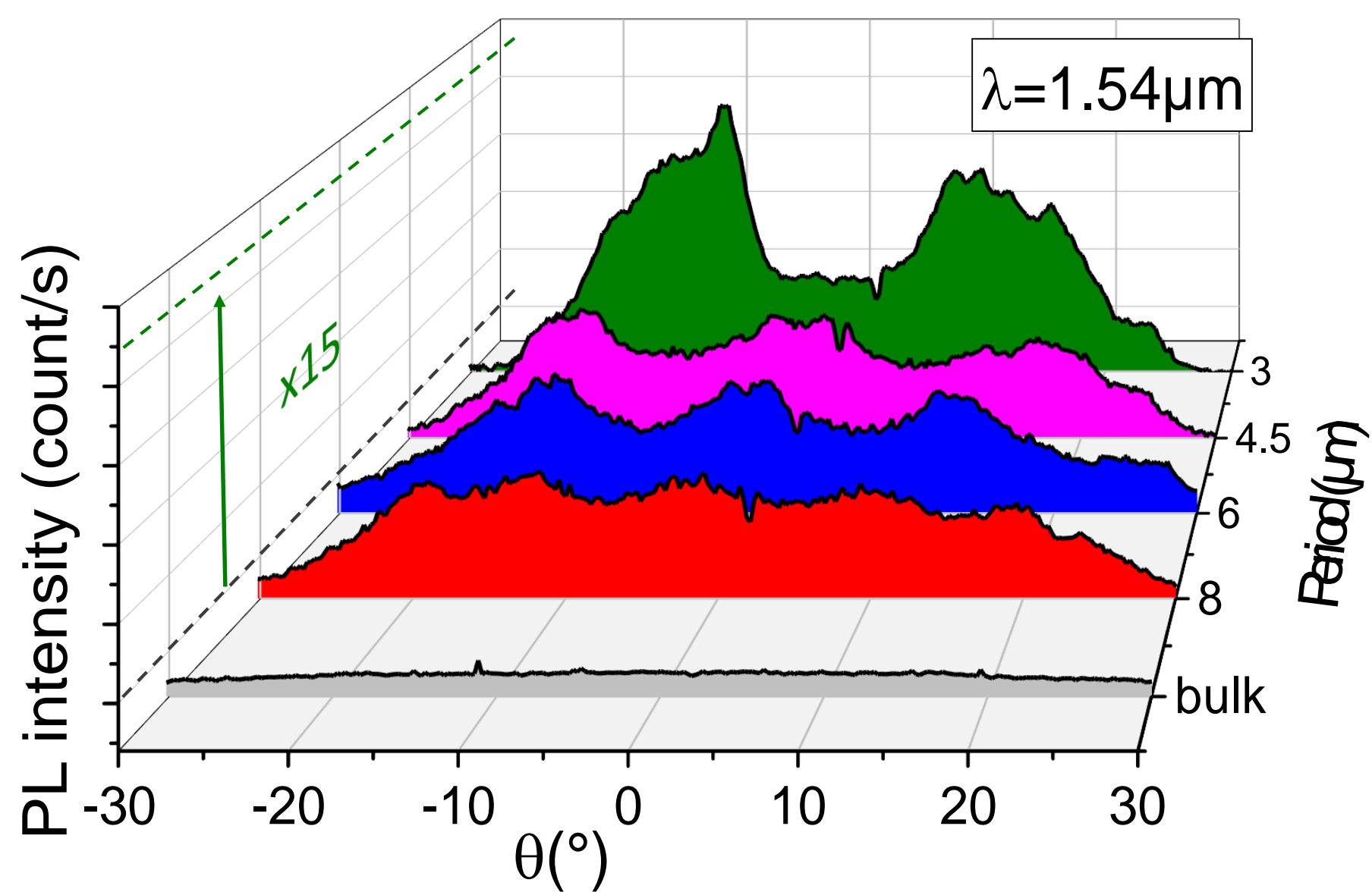
a)

 $p = 6\mu\text{m}$  – Far Field

b)



c)



d)

